Supporting Information

Synthesis of Cheeses-shaped capacitive covalent organic framework for lithium ion batteries by microwave ultrasonic coupling

Yueji Cai,[a] Chao Yu,*[a] Xiang Zhu,[b] Fanggang Li,[a] Hu Zhou,[a] Chunfeng Meng,[a] Haiqun Chen,[c] Yingzhong Shen,[d] Xian Tao,[d] and Aihua Yuan*[a]

a School of Materials Science and Engineering, School of Environmental and Chemical Engineering; Jiangsu University of Science and Technology; Zhenjiang 212100, P. R. China

E-mail: aihua.yuan@just.edu.cn (A. Yuan), chao_yu@just.edu.cn

b State Key Laboratory for Oxo Synthesis and Selective Oxidation

Suzhou Research Institute of Lanzhou Institute of Chemical Physics; Chinese Academy of Sciences

Suzhou 215000, P. R. China

c School of Petrochemical Engineering; Changzhou University

Changzhou, Jiangsu,213164, P.R. China

d Jiangsu MO Opto-Electronic Material CO., Ltd

Zhenjiang 212006, P. R. China.

Experimental section

Synthesis of HS. Firstly, 2,3,6,7,10,11-hexaiminotriphenylene (HITP) hexahydrochloride (21.5 mg) and benzoquinone (6.4 mg) were filled into a 25 mL boiling flask, and dry DMF (2 mL) was added under a nitrogen atmosphere. The boiling flask was violently agitated to achieve complete dissolution of HITP and benzoquinone with stirring at room temperature. Then, 5 M formic acid was added dropwise to the solution. After addition of formic acid, the boiling flask was heated at 150°C under a nitrogen atmosphere. Dark-red precipitates were collected by filtration after 24 h and washed with $NaHCO_3$, DI water and methanol. After that, Soxhlet extraction with water and methanol for 1 day each was carried out. The sample was dried at 50°C under reduced pressure (0.01 mm Hg) overnight to afford a dark-red powder.

Synthesis of Mw-n. Mw-n was prepared in a DMF mixture containing p-benzoquinone and HITP. Formic acid plays a central role in the formation of imine-bonded COFs. The reaction was performed for only 4 h at n*100 W (n=1, 2, 3, 4, 5) microwave power.

Synthesis of Mw-n@U. Mw-n@U is prepared in a DMF mixture containing p-benzoquinone and HITP. Using formic acid as catalyst. The reaction was performed for only 4 h at n*100 W (n=2, 4) microwave power and ultrasound. After separation, the yield can reach 90%~95%.

Material Characterization. As-synthesized Mw-n and Mw-n@U electrodes at different state of charge were analyzed by X-ray diffraction (XRD) in the 2θ range 3°-35° at a scanning rate of 2° min^{-1} by an X-ray diffractometer with a Cu Kα radiation at 40 kV and 40 mA. A Bomen infrared spectrophotometer was used to record Fourier transform infrared (FTIR) spectra of the as-synthesized HS, Mw-n and Mw-n@U powder and at different state of charge in the wavenumber ranging from 4000 cm^{-1} to 400 cm^{-1} in transmission mode. The thermogravimetric analysis (TGA) of the TP-COF was carried out in N_2 at a heating rate of 10°C min^{-1} using a Pyris Diamond TG-DTA (PerkinElmer). Microstructure and morphology of the synthesized TP-COF were investigated by a Zeiss Merlin Compact field emission scanning electron microscope (FESEM) and a transmission electron microscope (TEM) operating at 300 kV. the N_2 adsorption-desorption isotherms analysis for surface area measurements were carried out at 77.3 K using a Quantachrome Autosorb surface analyzer.To understand the oxidation states of the central atom, X-ray photoelectron spectroscopy (XPS) (ThermoFisher Nexsa) analysis was performed with the synthesized HS, Mw-n and Mw-n@U. Brunauer-Emmett-Teller (BET) analysis: First extraction with water and methanol Soxhlet at 423.15 K, 1 day each. The samples were then dried in a vacuum oven at 393.15 K for 12 hours. Finally, after vacuum degassing at 423.15 K for 3 hours, the static capacity method was used to perform nitrogen absorption degassing and pore size analysis. N_2 adsorption-desorption isotherm were carried out using a Micromeritics 3-FLEX pore and surface area analyser. Adsorbate model Nitrogen (SF): Temperature 77.3 K; Molec. Wt.: 28.013; Atom Diameter: 0.304 nm; Cold Zone V: 5.27826 cc; Warm Zone V: 15.841 cc; Analysis gas: Nitrogen; Non-ideality: 6.58e-05 1/Torr; CellType: 9mm w/o rod; Analysis Time: 9:24 hr:min; Bath temp.: 77.35 K. ^{13}C Solid-

State NMR Spectroscopy: High resolution solid-state NMR spectrum was recorded at ambient pressure on a Bruker AVANCE III spectrometer using a standard CP-TOSS pulse sequence (cross polarization with total suppression of sidebands) probe with 4 mm (outside diameter) zirconia rotors. Cross-polarization with TOSS was used to acquire ^{13}C data at 100.37 MHz. The ^{13}C ninety degree pulse widths were 4 μs. The decoupling frequency corresponded to 72 kHz. The TOSS sample-spinning rate was 5 kHz. Recycle delays was 2s.

Stability Test. The COF samples (100 mg) were soaked in different solvents including water, methanol, tetrahydrofuran (THF), aqueous HCl (1 M) and NaOH (1 M) solutions. These mixtures were stirred for one week. Before PXRD and nitrogen sorption isotherm measurements, the treated COF samples were successively washed with water, THF and methanol and then dried at 120 °C under vacuum for 12 h.

Electrochemical Measurement. Electrochemical properties of the prepared mixtures were evaluated by fabricating 2032 type coin cells versus Li/Li^+. For fabrication of the working electrodes, Mw-n and Mw-n@U, Super-P carbon, and polyvinylidene fluoride (PVDF) were homogeneously mixed in a weight ratio of 70:20:10 in N- methylpyrrolidone 9 μm thick copper foil (current collector) and dried in a vacuum oven at 120 °C for 12 h. After the coated foil was pressed at 4.0 ton inch 2, circular disks of 15 mm in diameter were cut and used as electrode. Typical active mass loading in the electrodes was 1.5-2.0 mg. Coin cells were assembled with these electrodes using Li metal as counter as well as reference electrode, $LiPF_6$ in EC/DMC (1:2 v/v) as electrolyte and Celgard 2300 as separator within an argon filled glovebox, where the moisture and oxygen levels were both kept below 0.5 ppm. Cyclic voltammetry of the cells was carried out by a electrochemical analyser (CHI600E) between 0.01 and 3.0 V at a scanning rate of 0.1 mV s^{-1}. Gavanostatic charge discharge measurements were carried out using LAND device(CT2001A, AC 220V, 50Hz, Wuhan LAND Electronic Co.Ltd.) in the same potential window. Electrochemical impedance spectra were recorded on a galvanostat potentiostat (PGSTAT302N, Autolab,The Netherlands) in the frequency range from 10 mHz to 1 MHz with an AC amplitude of 10 mV.

Computational details. First-principles calculations based on density functional theory (DFT) were performed using the plane-wave-based Vienna *ab initio* simulation package (VASP).[1, 2] The core valence interaction was examined using the projector augmented wave (PAW) method.[3] The exchange correlation potential was treated by the generalized gradient approximation (GGA) according to the scheme described by Perdew-Burke-Ernzerhof (PBE).[4] The cutoff energy for the plane-wave basis was set as 400 eV with the broadened Gaussian smearing[5] of 0.1 eV. The reciprocal space was sampled with a Monkhorst-Pack[6] *k*-point grid with resolution of 0.2 $Å^{-1}$. The vacuum region was set to 15 Å in the z direction to prevent the interaction between the neighboring slabs. The dipole corrections (IDIPOL= 3) were applied perpendicular to the surface. To account for van der Waals (vdW) interactions, the Grimme's DFT-D3 corrections[7] with BJ-damping were incorporated. The convergence of energy and forces were set as 1.0×10^{-6} and 0.005 eV/Å, respectively.

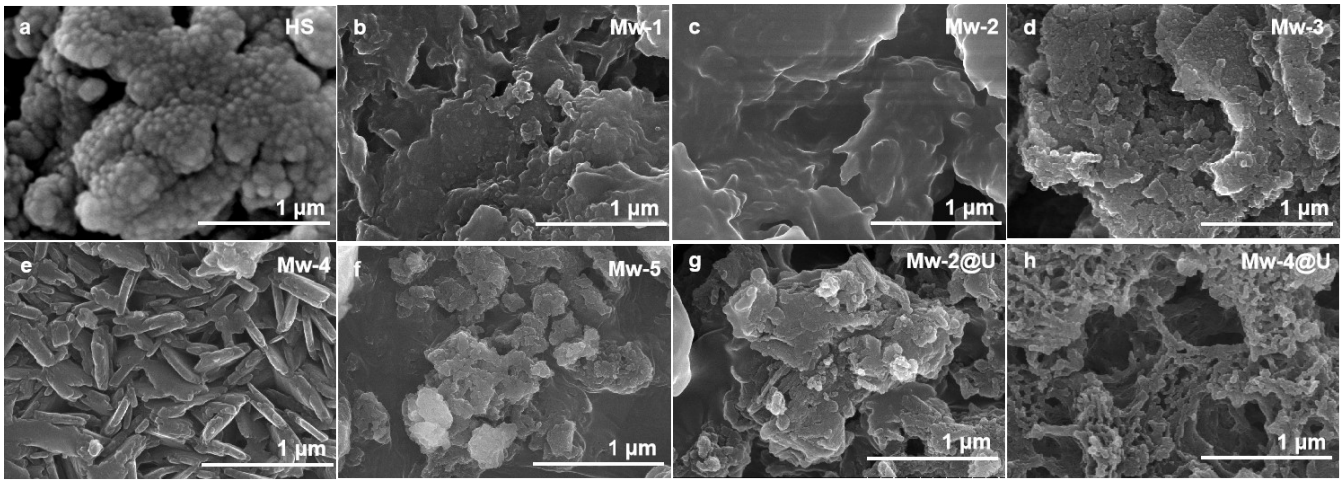

Fig. S1. (a-f) SEM images of HS and Mw-n (n=1-5); (g,h) SEM images of the Mw-2@U and Mw-4@U.

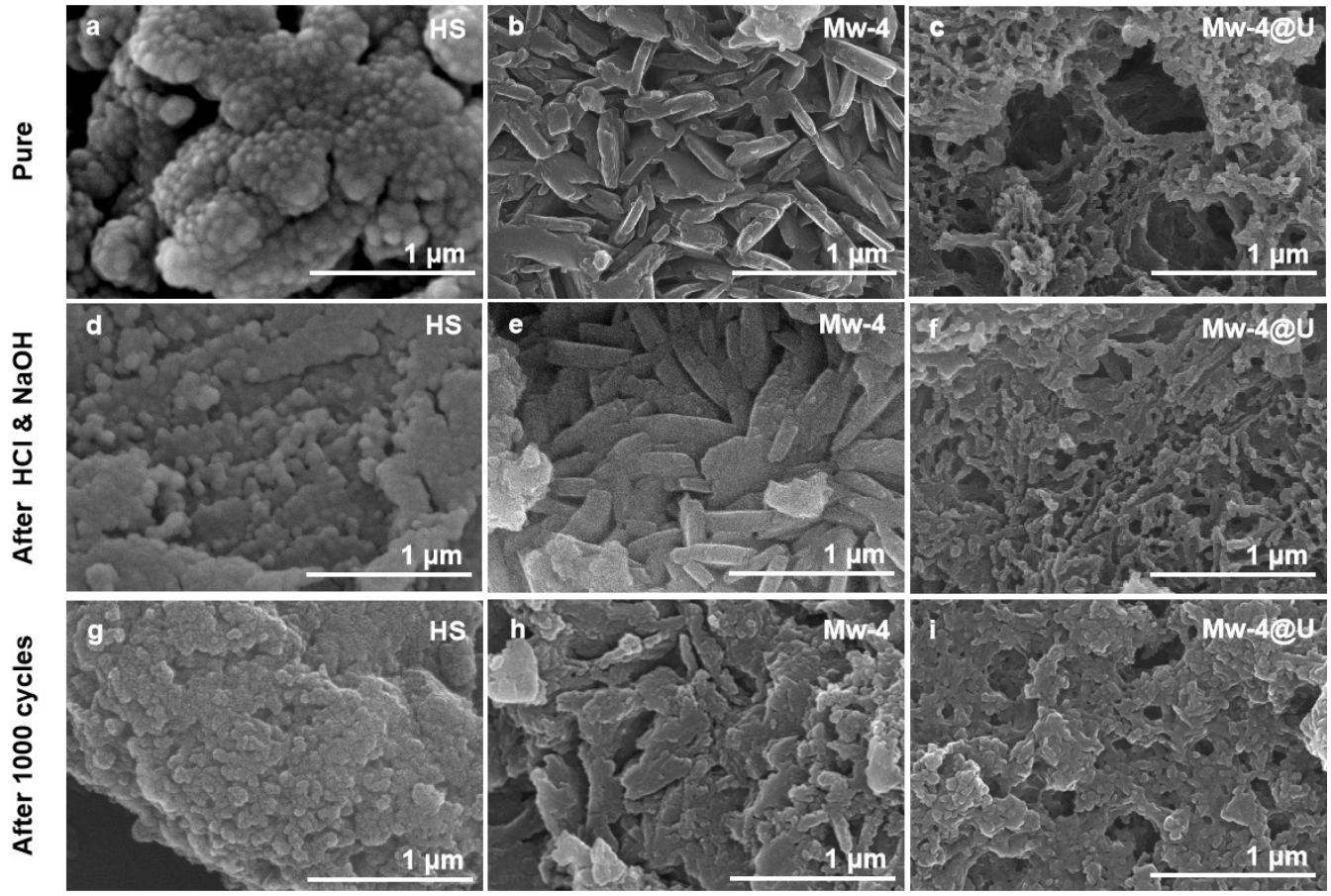

Fig. S2. (a-c) SEM images of HS, Mw-4 and Mw-4@U; (d-f) SEM images of HS, Mw-4 and Mw-4@U after soaked in different solutions, including water, methanol, THF, HCl (1 M) and NaOH (1 M) solutions, respectively; (g-i) SEM images of HS, Mw-4 and Mw-4@U after charging and discharging over 1000 cycles at the rate of 1 A g^{-1}, respectively.

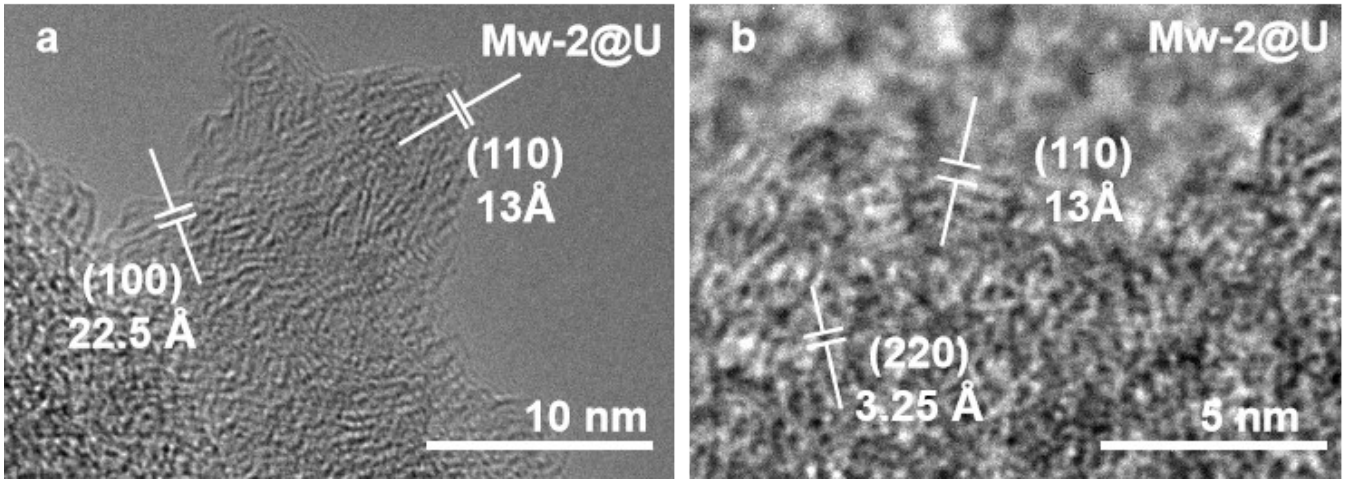

Fig. S3. (a,b) The HRTEM images of Mw-2@U.

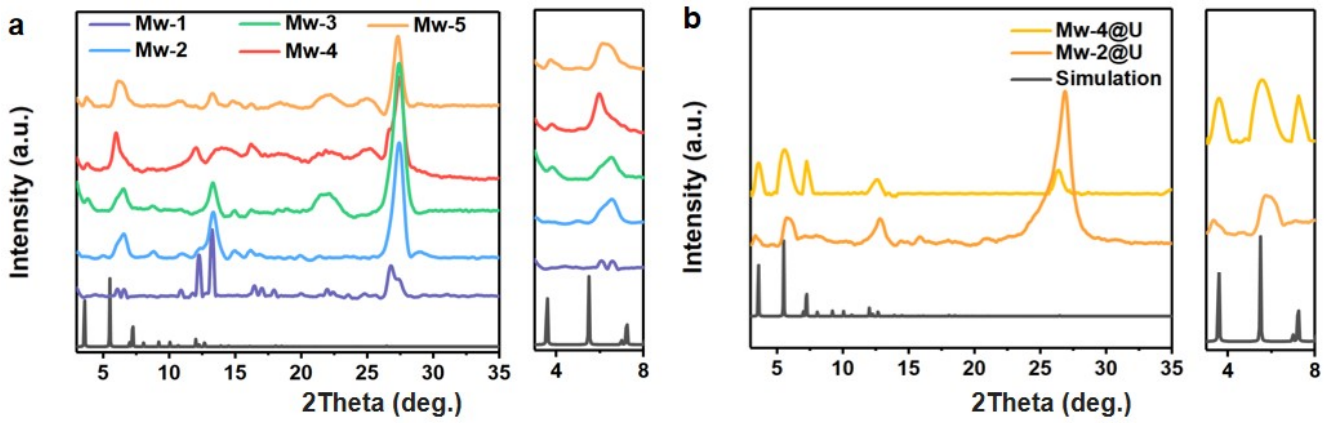

Fig. S4. XRD patterns of (a) Mw-n (n=1, 2, 4, 3, 5) and (b) Mw-2@U, Mw-4@U.

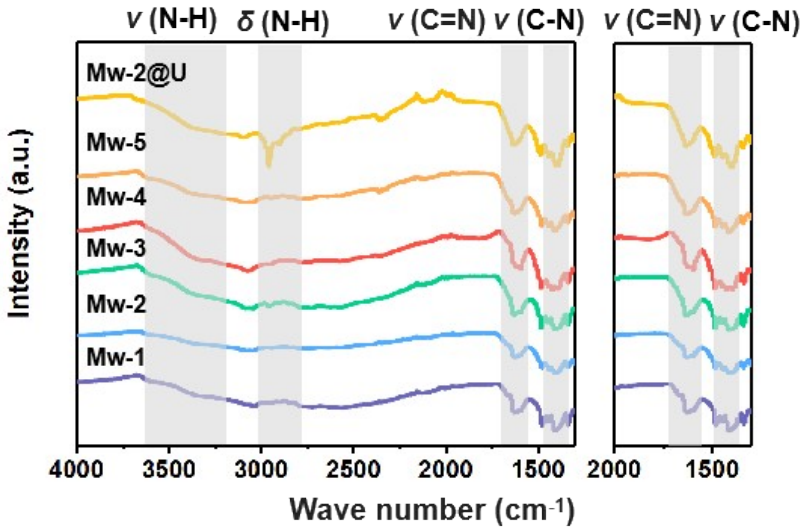

Fig. S5. FTIR spectra of a series of Mw-n (n=1, 2, 3, 4, 5) and Mw-2@U.

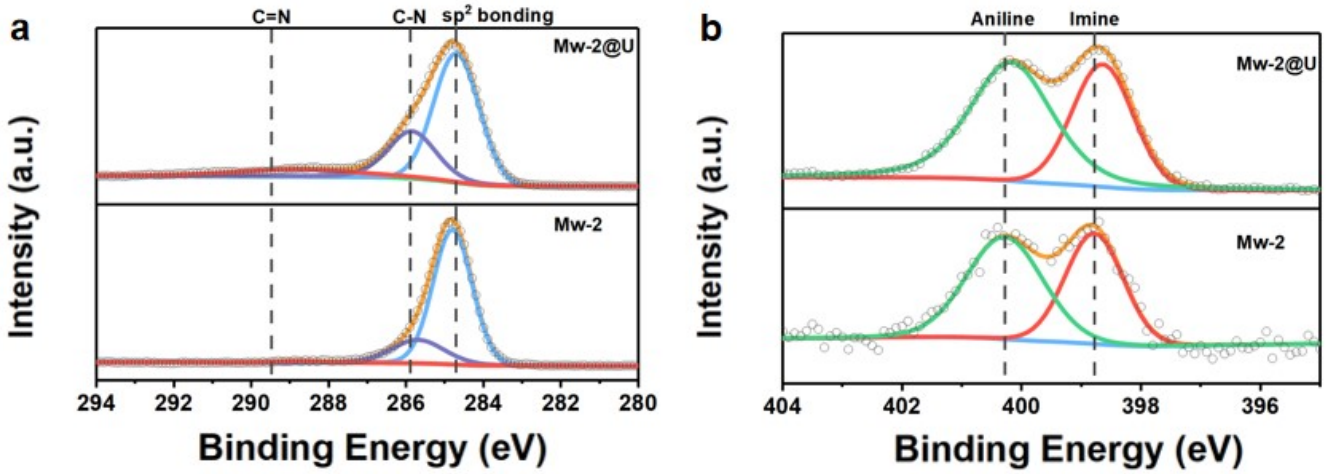

Fig. S6. (a,b) High-resolution XPS spectra of C 1s and N 1s on Mw-2 and Mw-2@U.

Table S1. The solid-state ^{13}C CP-MAS NMR spectrum revealed of chemical shifts

Assignment	Signal (ppm)	Comments
6	143	Aromatic C=N carbon
3, 4, 5	136	Aromatic C－N carbon
1	128	Aromatic C－C carbon
2	114	Aromatic C－H carbon
7	109	Aromatic C－H carbon

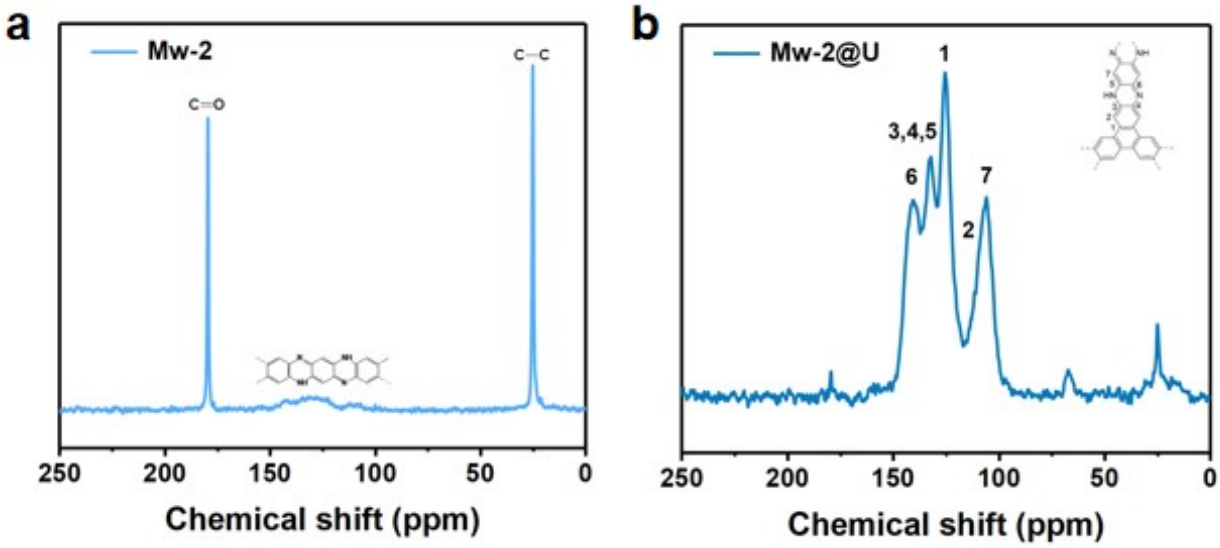

Fig. S7. (a,b) Solid state ^{13}C CP-MAS NMR spectra of Mw-2 and Mw-2@U.

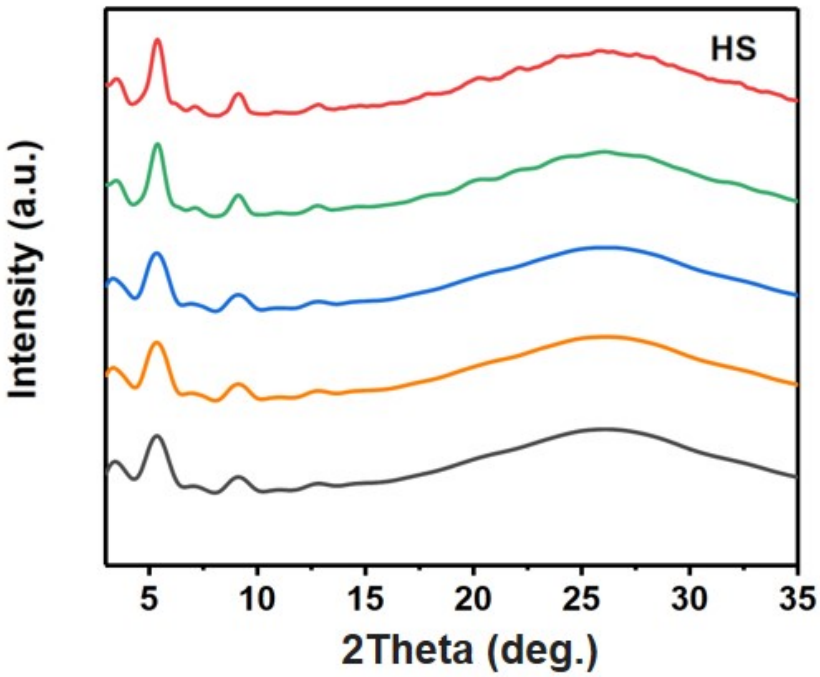

Fig. S8. XRD patterns of HS after soaking in water (red curve), methanol (green curve), THF (blue curve), HCl (1 mol L^{-1}, orange curve), and NaOH (1 mol L^{-1}, black curve).

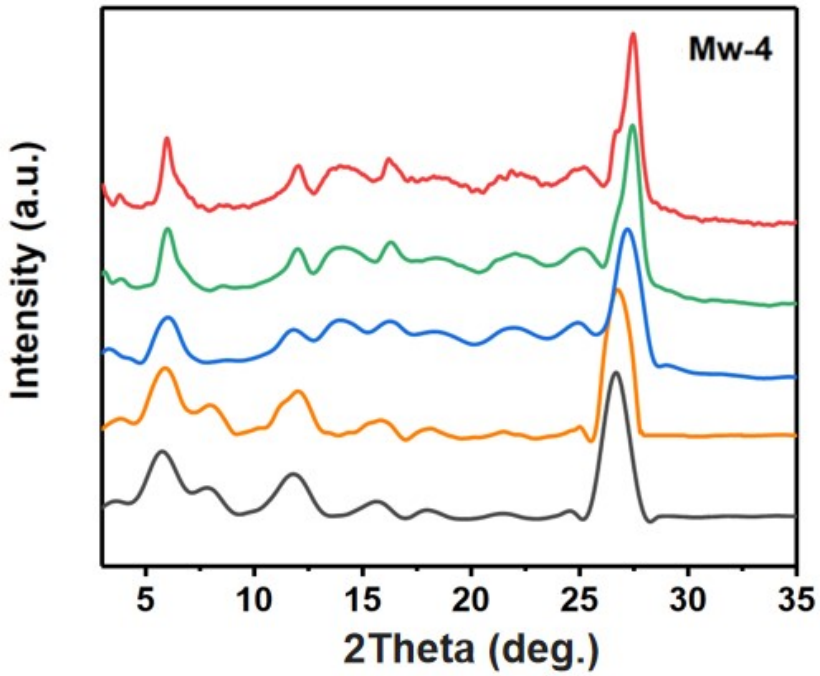

Fig. S9. XRD patterns of Mw-4 after soaking in water (red curve), methanol (green curve), THF (blue curve), HCl (1 mol L^{-1}, orange curve), and NaOH (1 mol L^{-1}, black curve).

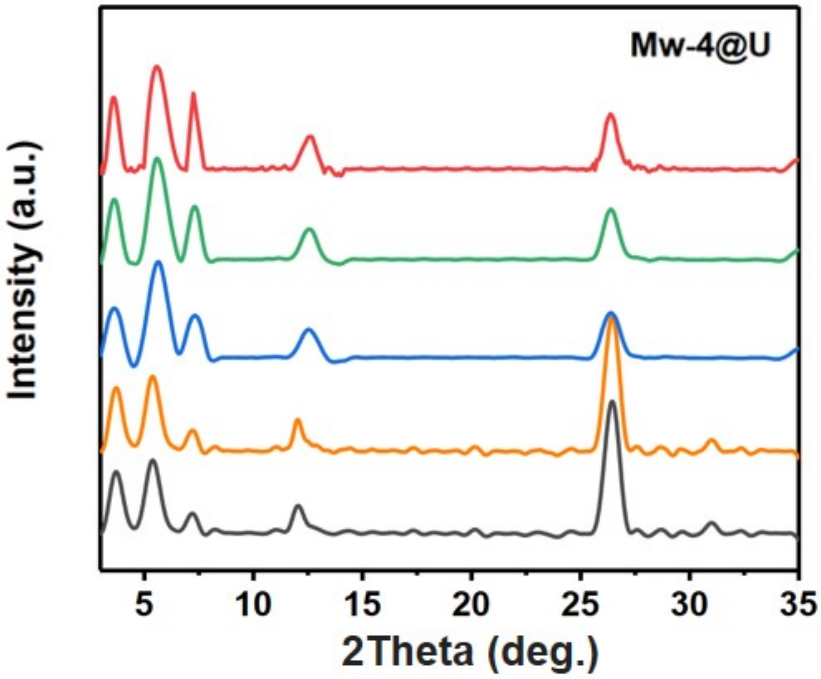

Fig. S10. XRD patterns of Mw-4@U after soaking in water (red curve), methanol (green curve), THF (blue curve), HCl (1 mol L^{-1}, orange curve), and NaOH (1 mol L^{-1}, black curve).

Table S2. Residual weight of HS, Mw-4 and Mw-4@U after treatment in different solutions.

Sample	Conditions	Residual weight (%)
HS	water	99.98
	methanol	99.98
	THF	99.97
	HCl (1 M)	99.95
	NaOH (1 M)	99.76
Mw-4	water	99.98
	methanol	99.91
	THF	99.98
	HCl (1 M)	99.74
	NaOH (1 M)	99.91
Mw-4@U	water	99.95
	methanol	99.96
	THF	99.95
	HCl (1 M)	99.92
	NaOH (1 M)	99.86

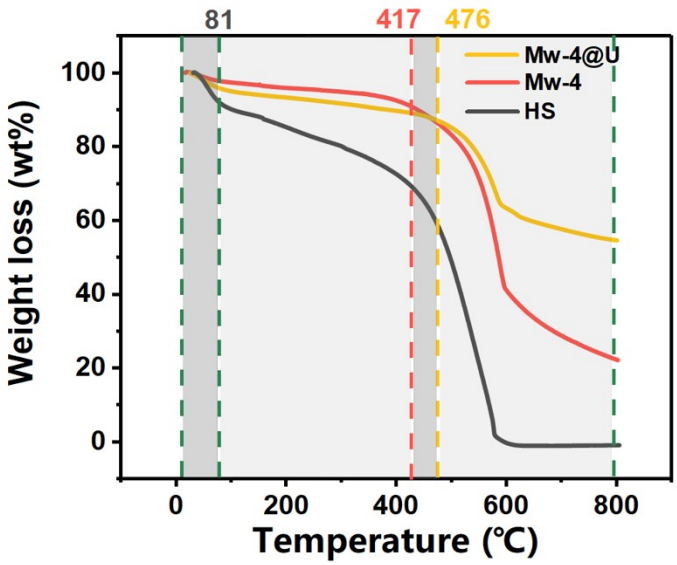

Fig. S11. Thermogravimetric analysis (TGA) of HS, Mw-4 and Mw-4@U.

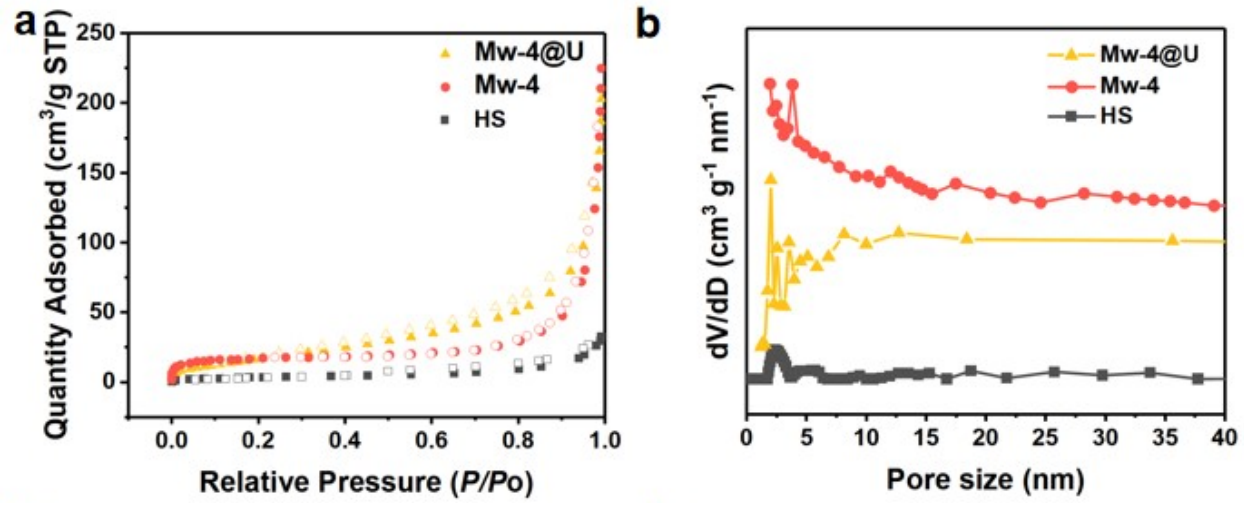

Fig. S12. (a) N_2 adsorption-desorption isotherm of HS, Mw-4 and Mw-4@U; (b) The pore size distributions of HS, Mw-4 and Mw-4@U.

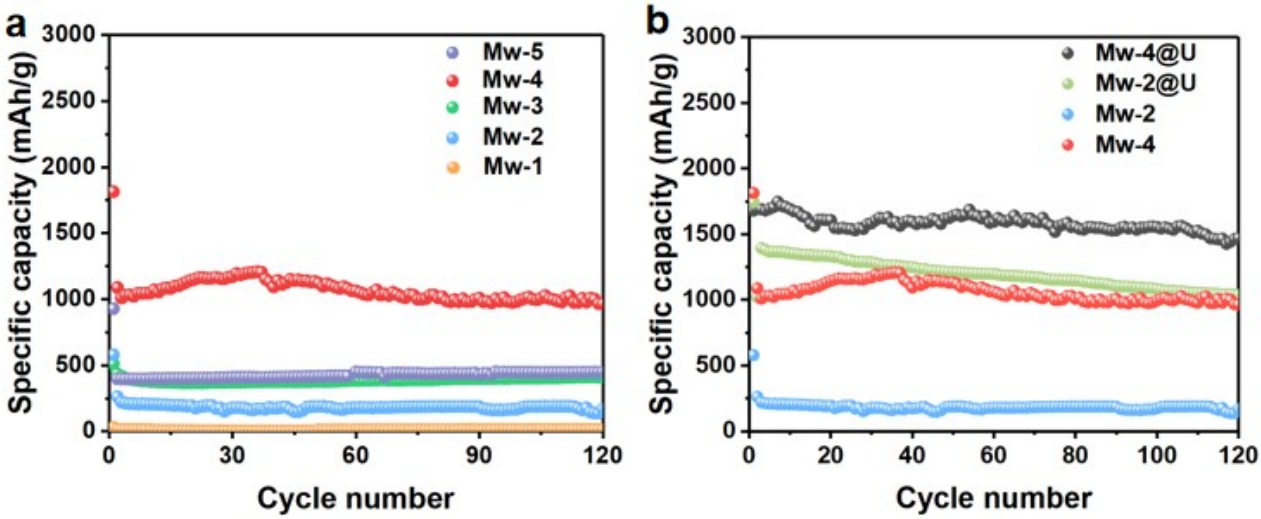

Fig. S13. (a) Cycling performance of Mw-n (n=1-5) over 120 cycles at 0.1 A g^{-1}; (b) Cycling performance of Mw-2, Mw-4, Mw-2@U and Mw-4@U over 120 cycles at 0.1 A g^{-1}.

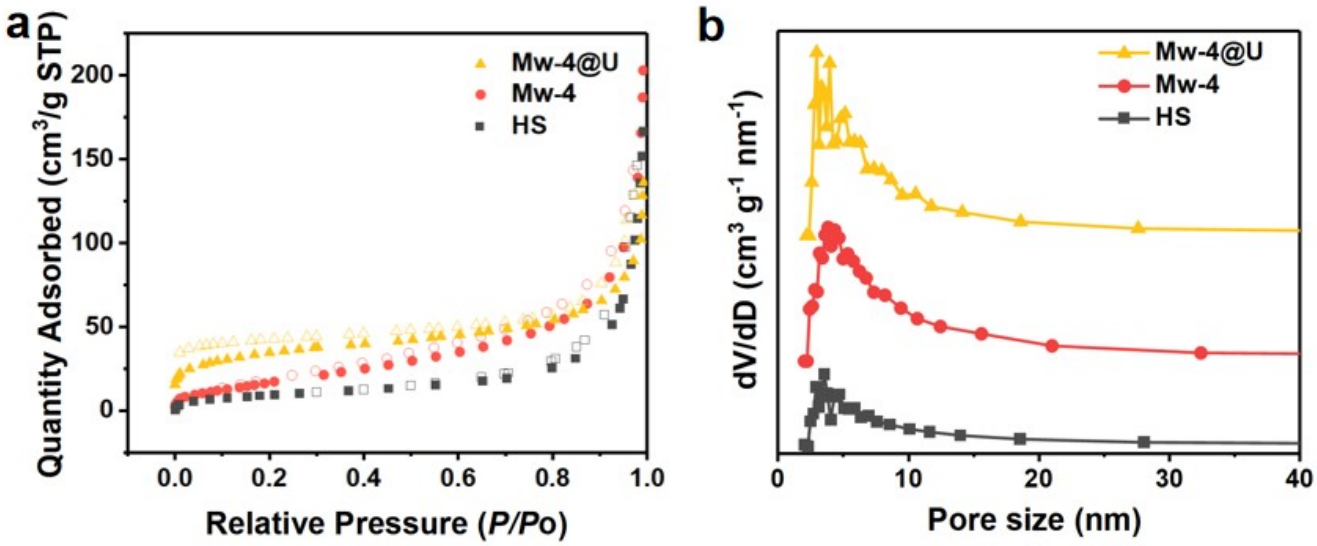

Fig. S14. HS, Mw-4 and Mw-4@U after charging and discharging over 1000 cycles at the rate of 1 A g^{-1}, respectively; (a) N_2 adsorption-desorption isotherm; (b) The pore size distributions.

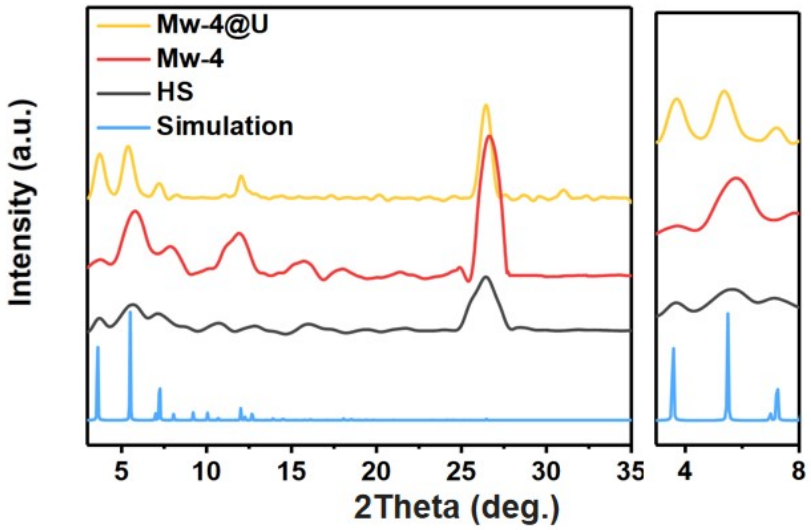

Fig. S15. HS, Mw-4 and Mw-4@U after charging and discharging over 1000 cycles at the rate of 1 A g^{-1}, respectively; (a) N_2 adsorption-desorption isotherm; (b) The pore size distributions.

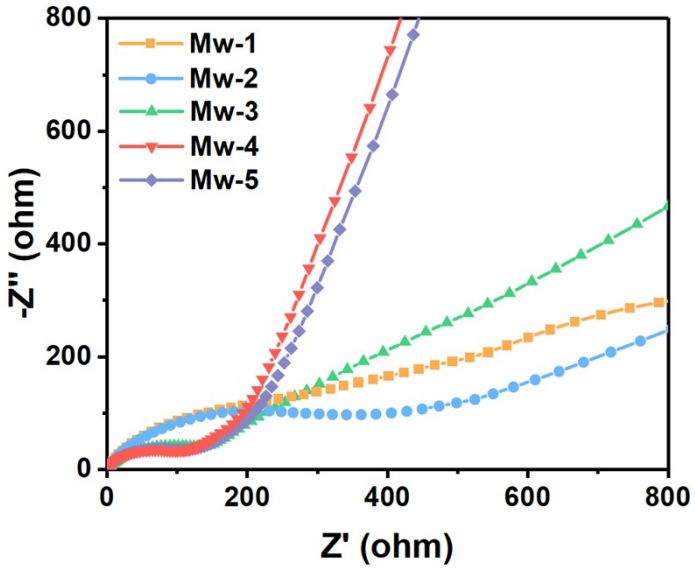

Fig. S16. Impedance spectra of Mw-n(n=1, 2, 3, 4, 5) electrodes.

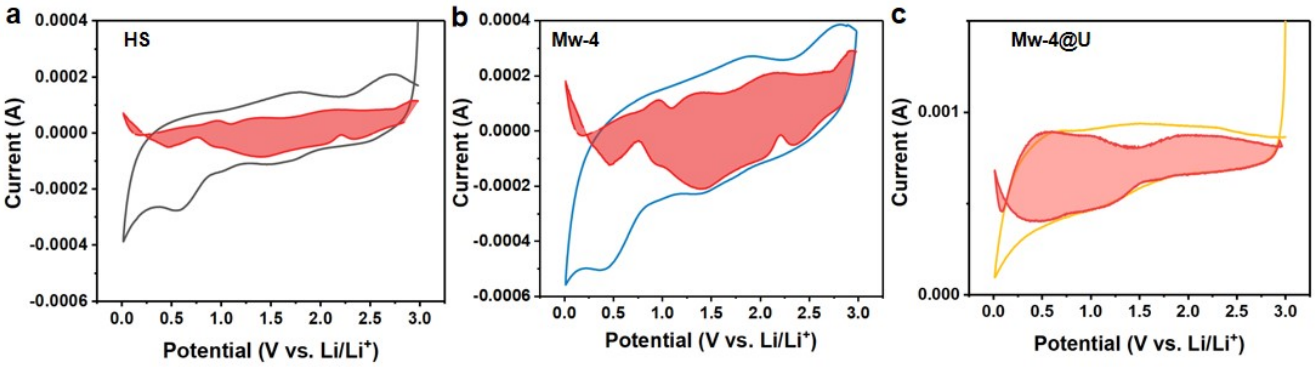

Fig. S17. Capacitive contributions of (a) HS, (b) Mw-4 and (c) Mw-4@U at 1.0 mV s^{-1}.

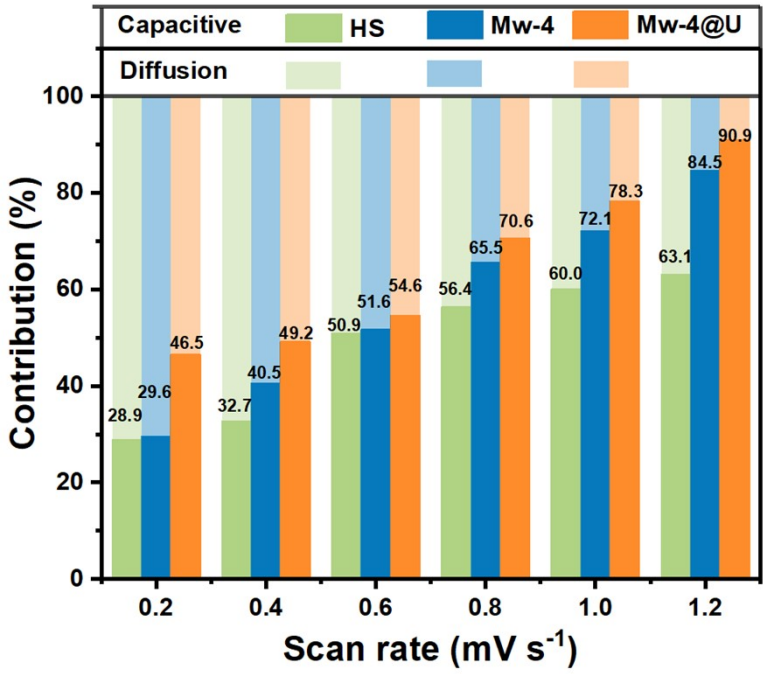

Fig. S18. Relative contributions of the capacitive and diffusion-controlled behavior at different scan rates.

Table S3. Comparison of discharge capacities with some of the best COF anode reported.

Materials	Current Density (mA g^{-1})/C rate	Cycling performance (cycles)	Specific Capacity (mA h g^{-1})	Ref.
Mw-4@U	100/1000	120/1000	1469.7/234.9	This work
TpBpy	1000	100	365	[8]
Ce-FeO@NC	100/1000	500	923.7/662.2	[9]
COF@Si	2000	1000	1864	[10]
TAACOF	500/10000	800/800	1035.7/548	[11]
E-TFPB-COF	100	300	968	[12]
TFPB-COF/MnO_2	2000	300	1359	[12]
COF-GQDs	100	300	820	[13]
COF	100	300	186	[14]
COF@CNTs	100	300	1536	[14]

Tp-Azo-COF	1000	3000	305.97	[15]
NBC-900	5000	1000	205.5	[16]
E-FCTF	100/200/500/1000/2000	1000	886/845/771/709/593	[17]

Table S4. optimized adsorption energy of Li complexes with TP-COF .

Assignment	Total energy (eV)	TP-COF energy (eV)	Li energy (eV)	Adsorption energy (eV)
N site	-682.43519	-680.45621	-0.06727	-1.91171
C site in phene sheet	-682.09395	-680.45515	-0.06638	-1.57242

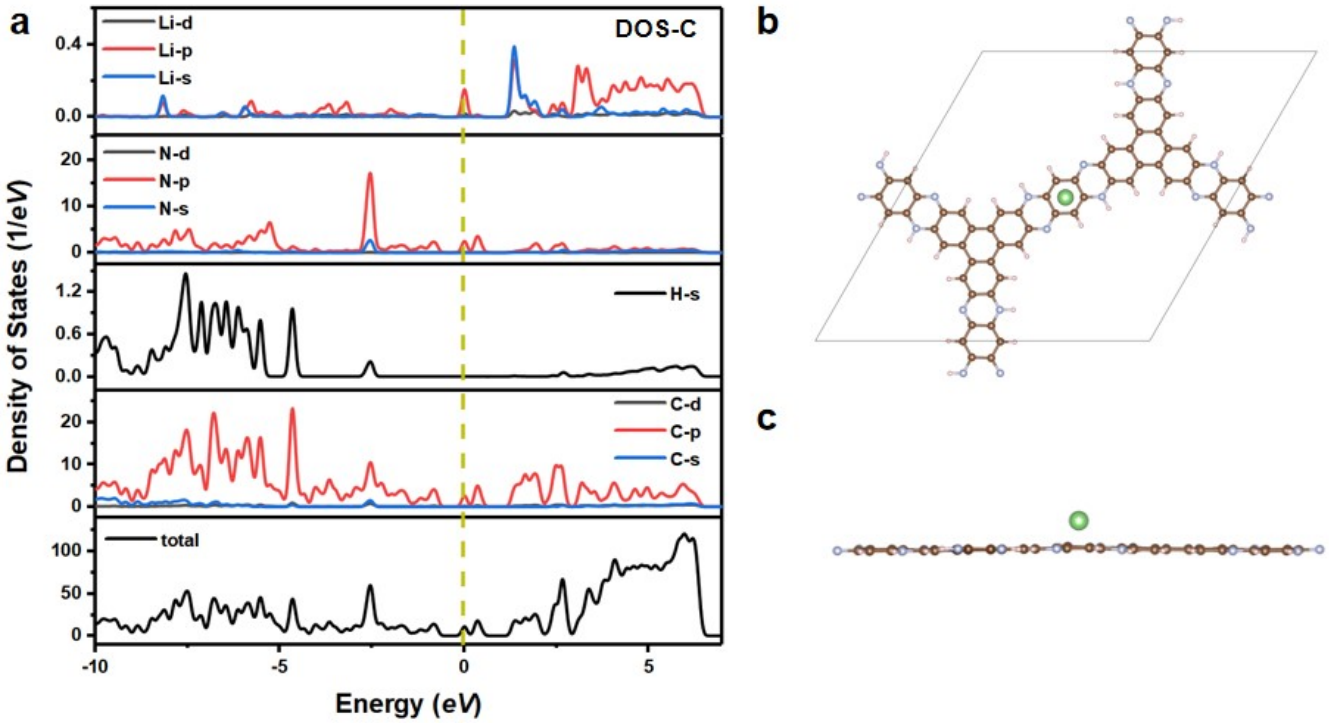

Fig. S19. (a) Calculated density of states (DOS) of C sites in TP-COF; (b) Top view of the atomic structures of the unit cell models of the TP-COF. Li adsorption at C sites; (c) side view of the atomic structures of the unit cell models of the TP-COF. Li adsorption at C sites.

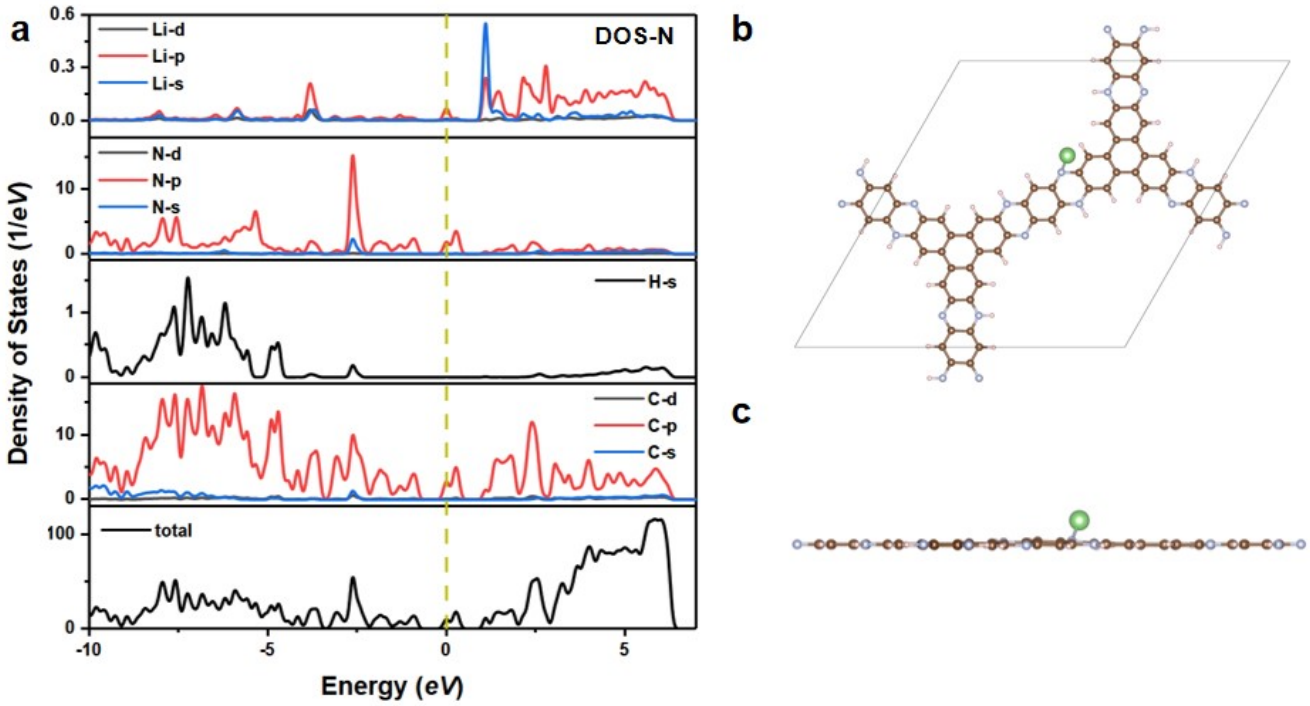

Fig. S20. (a) Calculated density of states (DOS) N sites in TP-COF; (b) Top view of the atomic structures of the unit cell models of the TP-COF. Li adsorption at N sites; (c) side view of the atomic structures of the unit cell models of the TP-COF. Li adsorption at N sites.

References

1. G. Kresse, and J. Furthmüller, *Computational Materials Science* **1996**, *6*, 15.

2. G. Kresse and D. Joubert, *Physical Review B,* **1999,** *59*, 1758.

3. P. E. Blöchl, *Physical Review B* **1994**, *50*, 17953.

4 J. P. Perdew, K. Burke, and M. Ernzerhof, *Physical Review Letters*, **1996,** *77*, 3865.

5. M. Methfessel, and A. T. Paxton, *Physical Review B* **1989,** *40*, 3616**.**

6. J. D. Pack, and H. J. Monkhorst, *Physical Review B* **1977**, *16*, 1748.

7 S. Grimme, Journal of Computational Chemistry, **2006,** 27, 1787.

8 S. Zhong, H. Zhao, Y. Ji, X. Li, T. Shu, Z. Cui and S. Liao, *J. Mater. Chem. A*, **2024**, *12*, 11571-11579.

9 Y. Li, K. Chen, H. Yu, Y. Du, Y. Song, *J. Energy Storage,* **2024,** *83,* 110661.

10 Q. Ai, Q. Fang, J. Liang, X. Xu, T. Zhai, G. Gao, H. Guo, G. Han, L. C , J. Lou, *Nano Energy,* **2020** *72*, 104657

11 X. Li, W. Liu, Y. Wang, L. Lv, H. Feng, W. Huang, Y. Sun, W. Xiong, H. Zheng, *Chem. Eng. J.,* **2023**, *473,* 145310.

12 X. Chen, Y. Li, L. Wang, Y. i. Xu, A. Nie, Q. Li, F. Wu, W. Sun, X. Zhang, R. Vajtai, P.M. Ajayan, L. Chen, Y. Wang, *Adv. Mater*., **2019**, *31*, 1901640-1901652.

13 H. Wang, L. Zhao, X. Tang, L. Lv, W. Sun, Y. Wang, *Chem. Eur. J.* **2022**, *28*, e202103901.

14 Z. Lei, Q. Yang, Y. Xu, et al., *Nat. Commun.* **2018**, *9*, 576.

15 G. Zhao, Y. Zhang, Z. Gao, et al., *ACS Energy Lett.* **2020**, *5,* 1022-1031.

16 S. Haidar, K. Roy, S. Nandi, et al., *Adv. Energy Mater.* **2018**, *8*, 1702170.

17 H. Zhang, W. Sun, X. Chen, et al., *ACS Nano*, **2019**, *13*, 14252-14261.